A giant elliptical galaxy with a lightweight initial mass function*†

Russell J. Smith‡ and John R. Lucey

Department of Physics, University of Durham, Durham DH1 3LE, UK

ABSTRACT

We present new observations of the closest known strong-lensing galaxy, the $\sigma \approx 330\,\mathrm{km\,s^{-1}}$ giant elliptical ESO325−G004, made with the ESO Very Large Telescope. The low redshift of the lens ($z_{\mathrm{l}} = 0.035$) results in arcs being formed at a small fraction of the effective radius ($R_{\mathrm{Ein}} = 2.85\,\mathrm{arcsec} \approx R_{\mathrm{eff}}/4$). At such small radii, stars dominate the lensing mass, so that lensing provides a direct probe of the stellar mass-to-light ratio, with only small corrections needed for dark matter. However, the redshift of the galaxy lensed by ESO325−G004 was unknown until now, so the lensing mass was not securely determined. Using X-SHOOTER, we have detected multiple spectral lines, from two bright parts of the arc system, and measured a source redshift of $z_{\mathrm{s}} = 2.141$. Combined with lens modelling constraints, this yields a total mass inside the Einstein radius of $1.50 \pm 0.06 \times 10^{11}\,\mathrm{M_\odot}$. We estimate the range of possible contribution of dark matter to the lensing mass, using halo profile statistics from cosmological *N*-body simulations. Subtracting this component yields a stellar mass-to-light ratio for the lens of $M_*/L_{F814W} = 3.14^{+0.24}_{-0.42}\,(\mathrm{M/L})_{\odot,\,F814W}$. Using VIMOS, we have also obtained very high signal-to-noise spectroscopy for the lens galaxy. Fitting models to this spectrum confirms that ESO325−G004 has a very old stellar population. For a Milky-Way-like (Kroupa) initial mass function (IMF), the stellar population fit yields a predicted stellar mass-to-light ratio of $\Upsilon_{\mathrm{MW}} = 3.01 \pm 0.25\,(\mathrm{M/L})_{\odot,\,F814W}$. Hence, the mass attributable to stars with a Kroupa IMF is consistent with the lensing estimate. By contrast, a Salpeter (or heavier) IMF is disfavoured at the 99.8 per cent confidence level. A 'heavyweight' IMF, with a mass twice as large as the Kroupa case, is firmly excluded for this galaxy. Such an IMF has been proposed for more distant elliptical lenses, and also to explain strong dwarf-star-sensitive spectral features, in particular the Na I 8200 Å doublet. A FORS2 far-red spectrum shows that this feature is as strong in ESO325−G004 as it is in other high-σ ellipticals, suggesting tension between dwarf-star indicators and lensing-mass constraints for this galaxy.

Key words: gravitational lensing: strong – stars: luminosity function, mass function – galaxies: elliptical and lenticular, cD – galaxies: individual: ESO325−G004 – galaxies: stellar content.

1 INTRODUCTION

The distribution of stellar masses at formation (the initial mass function, IMF) is a crucial quantity in astrophysics, both as a constraint on star-formation processes and in linking observed luminosities to the stellar masses of galaxies. It is therefore of great importance to establish whether the IMF is universal or, if not, how it depends systematically on the environment in which stars form.

Within the Milky Way (MW) and its satellites, the IMF can be determined directly through star counts. The distribution follows a power law with the Salpeter (1955) slope ($\mathrm{d}N(M) \propto M^{-x}\mathrm{d}M$ with $x = 2.35$) for $M \gtrsim 0.5\,\mathrm{M_\odot}$, but breaks to a shallower slope at lower mass (e.g. Kroupa 2001; Chabrier 2003). There is little evidence for systematic variation in IMF as a function of metallicity, star-formation rate or other properties in the MW itself (Bastian, Covey & Meyer 2010). However, IMFs with slopes flatter than Salpeter (at $\sim 0.7\,\mathrm{M_\odot}$) have been reported for several dwarf satellites, which probe to lower metallicities (Wyse et al. 2002; Geha et al. 2013; Kalirai et al. 2013).

For galaxies beyond the MW and its immediate neighbours, resolved star counts are impossible, and indirect methods are used. In this case, the mass-to-light ratio of the stellar population (M_*/L) provides a simple constraint on the IMF. For a single power law, slopes steeper than the Salpeter $x = 2.35$ imply large numbers of very faint dwarf stars which dominate the mass; for much flatter slopes, the mass budget becomes dominated by stellar remnants. In either case, M_*/L is increased relative to the Salpeter power law. Breaking the power law away from Salpeter at low mass, as observed in the MW, yields lower M_*/L than a single power law, by ∼35 per cent. Combining rotation curves with stellar population models for a sample of spiral galaxies, Bell & de Jong (2001) found that a ∼30 per cent reduction in mass, relative to Salpeter, was required to avoid violating dynamical constraints on the total mass. Hence, a MW-like (Chabrier or Kroupa) IMF appears to be generic for spiral galaxies as a class.

For elliptical galaxies, constraining the IMF via M_*/L poses a greater challenge, since masses are more difficult to establish for dynamically hot systems. Strong gravitational lensing of background galaxies provides a powerful method to determine masses in these objects. Important progress has been made through the systematic assembly and follow-up of large samples of lenses, especially from the Sloan Lens ACS (SLACS) survey (Bolton et al. 2006). In the SLACS methodology, lenses are selected through the presence of anomalous emission lines in the galaxy spectrum due to the lensed source, and followed up with *Hubble Space Telescope* (*HST*) imaging. Modelling the lensing configuration provides the total projected mass within an aperture, while the velocity dispersion from SDSS spectroscopy yields an additional dynamical constraint, which allows the stellar contribution to be decoupled from the dark-matter halo. Analysing 56 SLACS lenses, Treu et al. (2010, hereafter T10) found that for a universal standard Navarro, Frenk & White (1996, NFW) halo, some 80 per cent of the total lensing mass was contributed by the 'stellar' model component. Comparing the lensing stellar mass against the mass determined from stellar population fits to broad-band colours, T10 found that Salpeter IMFs were favoured over MW-like distributions on average, and that the mass normalization of the IMF increases with galaxy velocity dispersion. For the most massive SLACS galaxies, with $\sigma > 300\,\mathrm{km\,s^{-1}}$, the analysis requires an IMF twice as heavy as the Kroupa IMF. Recent lensing analysis of massive spiral galaxies suggests that there are variations within such galaxies, with bulges having heavier IMFs than discs (Dutton et al. 2013). Dynamical modelling estimates for nearby ellipticals also indicate a larger M_*/L than expected for a MW IMF (e.g. Thomas et al. 2011; Wegner et al. 2012; Cappellari et al. 2013). In the largest of these studies (Cappellari et al.), the average excess for the most massive galaxies is compatible with the Salpeter IMF, rather than the more extreme forms required by SLACS. Note, however, that the dynamical studies include few galaxies with very high velocity dispersion $\sigma > 300\,\mathrm{km\,s^{-1}}$.

As noted above, large M_*/L ratios could arise either from an excess of faint dwarf stars in a 'bottom-heavy' IMF or from an excess of dark remnants in a 'top-heavy' IMF. The analysis of gravity-sensitive spectroscopic absorption features promises to distinguish between these cases, by isolating lines and bands characteristic of either dwarf or giant stars (Spinrad & Taylor 1971; Whitford 1977; Cohen 1978; Faber & French 1980; Carter, Visvanathan & Pickles 1986; Couture & Hardy 1993; Cenarro et al. 2003; Conroy & van Dokkum 2012a, hereafter CvD12a). This method, updated with modern spectral synthesis model ingredients, was applied to a small sample of massive ellipticals by van Dokkum & Conroy

(2010), who found strong dwarf-star features which could only be reproduced in models with a very bottom-heavy IMF. Following this work, a number of studies have confirmed an apparent excess of low-mass stars in massive ellipticals, compared to the MW (Conroy & van Dokkum 2012b, hereafter CvD12b; Smith, Lucey & Carter 2012; Spiniello et al. 2012, 2013; Ferreras et al. 2013; La Barbera et al. 2013). The degree of dwarf-star enrichment, and the strength of its dependence on galaxy mass, metallicity and other properties, is still not fully clear however. In general, analyses which include the Na I 8200 Å doublet feature have tended to find stronger evidence for dwarf enrichment, a discrepancy already noted by Carter et al. (1986), and persisting to the latest works (e.g. fig. 12 of CvD12b). A particular challenge is to decouple the IMF effect from trends in abundance ratios, especially Na/Fe which affects not only the Na I doublet but also many other lines, through its strong influence on the free electron pressure in cool stellar atmospheres (CvD12a). For the most massive ellipticals ($\sigma > 300\,\mathrm{km\,s^{-1}}$), CvD12b favour IMFs with mass normalization twice that of the MW IMF, in close concordance with the SLACS lensing results.

In summary, several recent studies have presented evidence for 'heavyweight' IMFs[1] in giant ellipticals, with a mass-to-light ratio twice that of a MW-like IMF. Given the important and widespread implications of this result, careful observational scrutiny is essential. In this paper, we exploit an unusual low-redshift lens system to measure the stellar mass-to-light ratio in a single, but very powerful, $\sigma > 300\,\mathrm{km\,s^{-1}}$ elliptical galaxy. In Smith et al. (2005, hereafter S05), we discovered a system of gravitationally lensed arcs around ESO325−G004, using *HST* imaging. This was a serendipitous discovery, in the sense that it was not derived from any systematic search for lenses. Due to the closeness of this lens ($z_l = 0.035$), the Einstein radius in ESO325−G004 is smaller than the stellar effective radius, by a factor of 4. Hence, in this system the lensing mass is dominated by stars to an unusual degree, and only small corrections for dark matter are required. However, the lensing mass has not been determined until now, because the redshift of the background source was unknown. In this paper, we report the measurement of the source redshift and determine the implications for the stellar mass-to-light ratio and IMF in ESO325−G004.

The structure of the paper is as follows. Section 2 presents the observations, including measurement of the source redshift (Section 2.1), photometry and determination of the total lensing mass (Section 2.2), and spectroscopy of the lens galaxy to determine its age, and hence the mass-to-light ratio expected for a given IMF (Section 2.3), In Section 3, we estimate the likely contribution of dark matter to the lensing mass. Section 4 compares the dark-matter-corrected lensing mass against the age constraints to infer the viable range of IMF normalization, and presents tests for the robustness of our analysis. In Section 5, we compare our results to those obtained from SLACS, and to the results from dwarf-star indicators, including a measurement of the Na I 8200 Å feature for ESO325−G004 itself. Brief conclusions are summarized in Section 6.

Where necessary, we adopt cosmological parameters from *Wilkinson Microwave Anisotropy Probe* 7 (*WMAP*7): $H_0 = 70.4\,\mathrm{km\,s^{-1}\,Mpc^{-1}}$, $\Omega_m = 0.272$ and $\Omega_\Lambda = 0.728$ (Komatsu et al. 2011).

---

[1] We use the term 'heavyweight' to refer to the high mass normalization, without reference to whether this arises from dwarf stars or from remnants.

2 OBSERVATIONS

2.1 X-SHOOTER spectroscopy: arc redshift

We observed ESO325−G004 with the X-SHOOTER three-arm echelle spectrograph (Vernet et al. 2011), mounted on UT2 of the European Southern Observatory (ESO) Very Large Telescope (VLT), on 2013 March 7. Spectra were obtained with a 0.4 arcsec slit, providing resolving powers 10 000, 18 000 and 10 500 in the UVB, VIS and NIR arms, respectively. The total integration time was 2400 s, split between two exposures. The image quality, as estimated from the acquisition frames, was ∼0.5 arcsec full width at half-maximum (FWHM). The slit was aligned to intersect two segments of the arc system (Arc C and the brightest part of Arc A, in the nomenclature of S05), as shown in Fig. 1.

Visual inspection of the raw data revealed the presence of emission lines only in the NIR arm spectra. Identical line emission is observed from the two arc segments, confirming beyond reasonable doubt that the source is indeed a multiply imaged lensed galaxy (Fig. 2). The observations were reduced using the standard X-SHOOTER pipeline, to produce a rectified and wavelength-calibrated two-dimensional spectrum. An approximate correction for telluric absorption was applied using a standard star observation. One-dimensional sky-subtracted spectra were extracted centred on each arc and combined to yield the final spectrum, extracts from which are shown in Fig. 3. Despite the short total integration time and the small number of exposures (hence poor rejection of cosmetic defects), four emission lines are detected, at wavelengths corresponding to [O III] λλ 4594, 5007 Å, Hβ and Hα for a source redshift of $z_s = 2.141$. The characteristics of the lensed source are
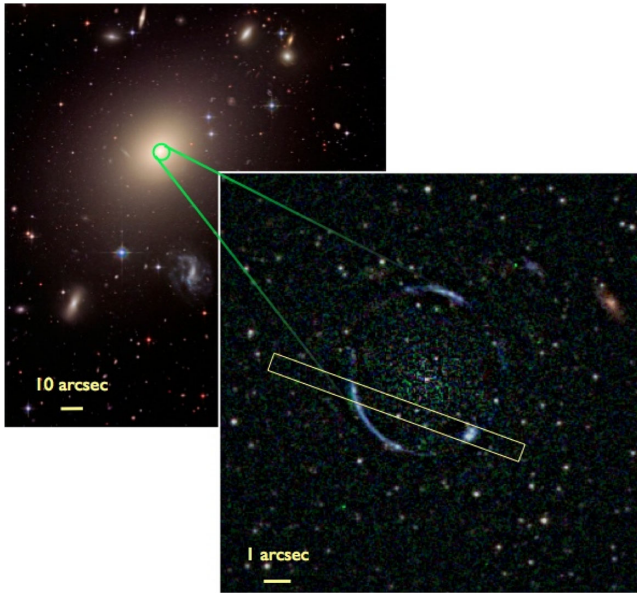
Figure 1. *HST* image of the $z = 0.035$ giant elliptical galaxy ESO325−G004 (S05) and its immediate environment (credit: NASA/ESA and the Hubble Heritage Team). The inset shows a zoom of the central regions of the image after subtracting a smooth model describing the lens galaxy. The arcs are formed at the Einstein radius of 2.85 arcsec (1.96 kpc at the distance of the lens). Because this is small compared to the effective radius (12.3 arcsec), the enclosed mass is dominated by stars, rather than dark matter (see Section 3). The coloured figures were created from *F*475*W* (blue, 4800 s exposure), *F*625*W* (green, 2400 s) and *F*814*W* (red, 18900 s) images taken with the Advanced Camera for Surveys. The yellow rectangle indicates the slit orientation for the X-SHOOTER observations.

not the concern of this paper, but we note that the spectrum is similar to those of other lensed high-redshift star-forming galaxies (Richard et al. 2011).

2.2 *HST* photometry and lensing analysis

ESO325−G004 was originally observed with the Advanced Camera for Surveys (ACS) on *HST* in 2005 January (programme 10429, P.I. Blakeslee), for 18 900 s in *F*814*W* and 1100 s in *F*475*W*, as reported by S05. Deeper observations in blue passbands were obtained in 2006 February (programme 10710, P.I. Noll) for a Hubble Heritage public release, providing 4800 s in *F*475*W* and 2400 s in *F*625*W*.

The lensing mass was determined by S05, modulo the then-unknown source redshift, using a singular isothermal sphere (SIS) model with an additional external shear term. From this model, S05 found an Einstein radius of $R_{\rm Ein} = 2.85$ arcsec and a corresponding mass (projected within $R_{\rm Ein}$) of $M_{\rm Ein}^{\rm SIS} = 1.40 \times 10^{11}(D_s/D_{ls})$ M$_\odot$. Here, D_s is the angular-diameter distance from the observer to the source and D_{ls} is the angular-diameter distance from the lens to the source. For the measured source redshift $z_{\rm src} = 2.141$, the geometric factor is close to unity, $D_s/D_{ls} = 1.027$ (with negligible error). Hence, the lensing mass for the SIS model is $M_{\rm Ein}^{\rm SIS} = 1.44 \times 10^{11}$ M$_\odot$. The effective (half-light) radius of ESO325−G004, determined from the *F*814*W* image is $R_{\rm eff} = 12.3 \pm 0.5$ arcsec, a factor of 4 larger than $R_{\rm Ein}$.

We derive the luminosity projected within the Einstein radius from simple aperture photometry performed on the *HST*/ACS in *F*814*W* and *F*475*W* filters.[2] We work entirely in the native photometric bandpasses, at the observed redshift of ESO325−G004, and express all magnitudes in the Vega system. The observed aperture magnitudes are *F*814*W* = 13.543 and *F*475*W* = 15.568. Extinction corrections are $A_{F814W} = 0.092$ and $A_{F475W} = 0.196$, from Schlafly & Finkbeiner (2011). We assume a luminosity distance of 152 Mpc (*WMAP*7 cosmology, no peculiar velocity), and hence a distance modulus of 35.909 mag. The absolute magnitude of the Sun, redshifted to $z = 0.034$ in the observed bands, is 4.066 in *F*814*W* and 5.254 in *F*475*W* (determined using EZGAL; Mancone & Gonzalez 2012). Hence, the luminosities are $L_{F814W} = 4.07 \times 10^{10}$ L$_{\odot, F814W}$ and $L_{F475W} = 2.07 \times 10^{10}$ L$_{\odot, F475W}$. We adopt a 2 per cent error on luminosity to account for absolute calibration uncertainties (the statistical errors are much smaller). The ratio of SIS lensing mass to luminosity gives the total $M_{\rm Ein}^{\rm SIS}/L_{F814W} = 3.54 \pm 0.06$ (M/L)$_\odot$.

Since the ESO325−G004 lensing mass is expected to be dominated by stellar mass, rather than by dark matter (see Section 3), we have also modelled the lensing configuration using a mass distribution proportional to the observed luminosity. To fit this mass-follows-light (MFL) model, we treat the lens as a set of point masses and compute the net deflection experienced by image-plane pixels corresponding to the arcs (as identified in the deep *F*475*W* image). For the 'mass' image, we use a smooth model derived from ellipse fitting to the *F*814*W* image, and incorporating harmonic terms to describe the slightly boxy isophote shape. The lens model is then specified by the (total) mass-to-light ratio M/L, plus a linear shear term, with free amplitude and direction, intended to account for additional distortions due to nearby structures. Given values for these parameters, we determine the source-plane location of the

---

[2] The transformation to Johnson–Cousins magnitudes applied in S05 was erroneous, leading to a mass-to-light ratio substantially lower than we report here.
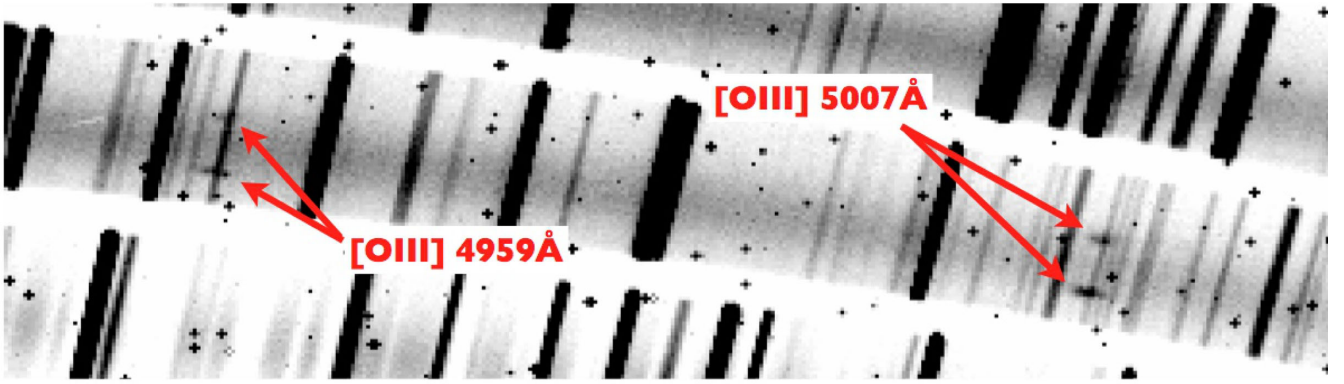
Figure 2. Extract from the raw, two-dimensional spectrum from a single X-SHOOTER NIR exposure, showing the redshifted [O III] lines from the lensed source. The slit was aligned to intersect two arcs (see Fig. 1); lines from both are clearly visible, on either side of the diffuse trace of the lens-galaxy continuum.
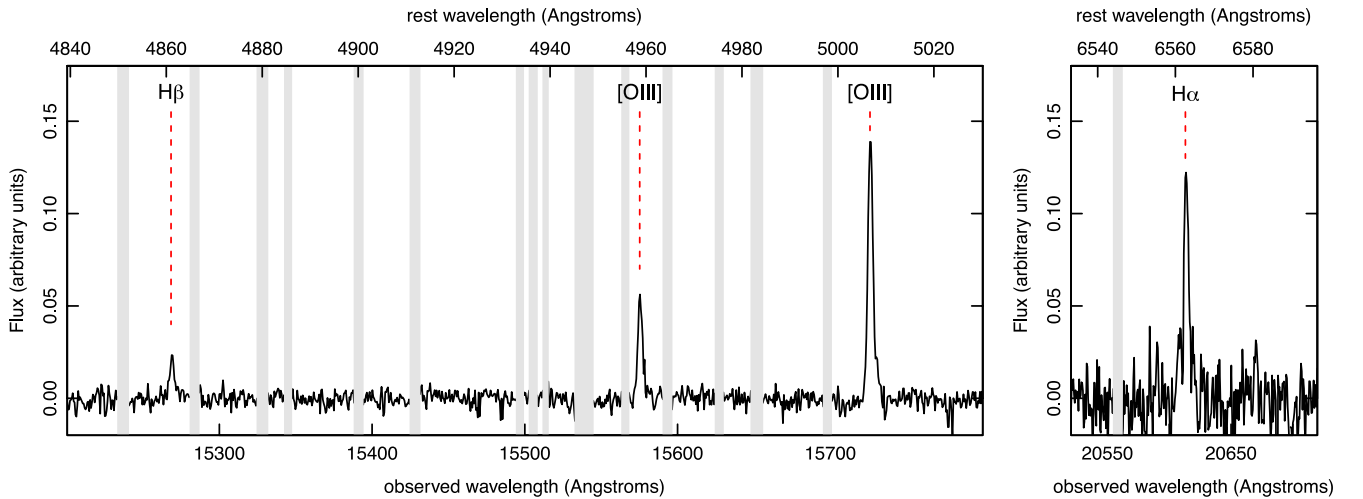
Figure 3. Segments of the one-dimensional spectrum of the lensed source. The signal has been combined over both arcs and both exposures. Areas affected by strong sky lines are masked in grey. A smooth background (including any true continuum) has been subtracted from the spectrum. Emission line positions are shown for a redshift of $z_s = 2.141$.

arc pixels, and their likelihood of being drawn from a single compact region on the source plane. The assumed intrinsic source is a circular Gaussian with 0.35 arcsec FWHM. Interpreting this likelihood as the probability that the lens model is correct, we use a Markov chain Monte Carlo method to sample from the probability distribution of the model parameters. Marginalizing over the shear amplitude and direction, this method yields $M_{\mathrm{Ein}}^{\mathrm{MFL}}/L_{F814W} = 3.69 \pm 0.06$, marginally larger than the SIS result. Hereafter, we adopt the results of the MFL for the lensing mass-to-light ratio, and the nominal Einstein radius is that derived from the SIS model. Thus, the mass within R_{Ein} is $M_{\mathrm{Ein}}^{\mathrm{MFL}} = 1.50 \times 10^{11}\,\mathrm{M}_{\odot}$, i.e. 4 per cent larger than found from the (oversimplistic) SIS model. Other lens models which account for the angular structure of the luminous matter (e.g. a singular isothermal ellipse, with or without external shear) yield similar M_{Ein} to the MFL approach, within ~1 per cent. The robustness of M_{Ein}, with respect to reasonable choices for the mass model, is a standard result in lensing studies (e.g. Kochanek 1991; Koopmans et al. 2006; Treu 2010). In principle, M_{Ein} includes contributions from all structures along the line of sight to the source; in Λ CDM cosmology, the rms contribution from large-scale structure is calculated to be ~2 per cent for a $z = 2$ source (Taruya et al. 2002).

In what follows, we adopt the lensing mass from the MFL model, $M_{\mathrm{Ein}} = 1.50 \pm 0.06 \times 10^{11}\,\mathrm{M}_{\odot}$. The adopted 4 per cent error reflects a conservative estimate of the systematic uncertainties, based on the difference between SIS- and MFL-model masses.

2.3 VIMOS spectroscopy: lens properties

The lensing M/L yields information on the IMF if other parameters of the stellar population, in particular its age, can be constrained using additional data.

We observed ESO325−G004 with VIMOS (Le Fevre et al. 2003) in integral-field unit (IFU) mode, on UT3 of the VLT in 2006 April–May. The data were obtained using the ('old') HR-blue grism, with a wavelength range of 4200–6200 Å and a resolution of 1.65 Å FWHM, sampled at 0.54 Å pixel^{-1}. The spatial coverage was 13×13 arcsec^2, with a scale of 0.33 arcsec per IFU fibre. Eight individual spectra were obtained, each with an integration time of 1865 s, with pointing adjustments of a few arcsec between observations to average over fibre sensitivity variations. The pipeline-reduced spectra from IFU elements within $R_{\mathrm{Ein}} = 2.85$ arcsec of the galaxy centre were combined from each observation separately to allow assessment of systematic errors between exposures. The

Table 1. Line-strength indices, as measured from the VIMOS spectrum, expressed in angstroms. Values in the third column have been corrected for velocity broadening and corrected to the Lick-system resolution and flux-response system. Errors were derived from the scatter among eight separate observations.

Index	Raw	Corrected
$H\beta$	1.68 ± 0.03	1.63 ± 0.03
$H\gamma_F$	-2.09 ± 0.08	-2.08 ± 0.08
Mgb	4.22 ± 0.04	4.90 ± 0.05
Fe5015	4.18 ± 0.10	5.29 ± 0.12
Fe5270	2.46 ± 0.05	2.92 ± 0.06
Fe5335	1.95 ± 0.04	2.83 ± 0.05

Figure 4. Determination of Υ_{MW}, i.e. the stellar mass-to-light ratio for a MW-like IMF, from spectroscopy of the lens. The grey-scale and red contours show the probability distribution (marginalized over $[\alpha/Fe]$) for the age and metallicity, derived from fits to the measured indices. The blue contours indicate the mass-to-light ratio (in $F814W$, labelled in solar units) corresponding to each location on the grid.
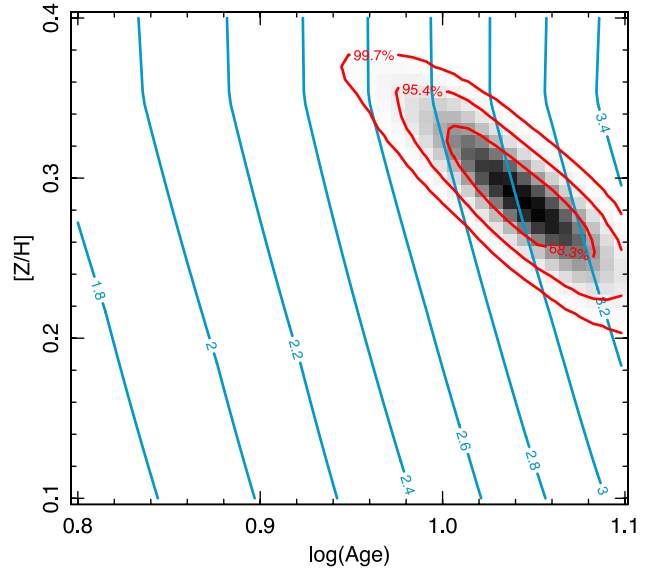
overall signal-to-noise (S/N) ratio for the full 4 h integration is $\sim 400 \, \text{Å}^{-1}$ at 5000 Å.

Standard Lick absorption indices were measured on the combined spectra and corrected to the standard Lick resolution (~ 9 Å FWHM, but wavelength dependent) and to zero velocity dispersion, following the method described in Smith, Lucey & Hudson (2007). The velocity dispersion measured from the extracted spectrum, and used for the resolution correction, is $\sigma = 335 \, \text{km s}^{-1}$. Corrections from the flux-calibrated system to the Lick flux-response system were applied using the offsets tabulated by Norris, Sharples & Kuntschner (2006). The index data are given in Table 1.

As may be expected given the very high S/N ratio, the scatter in index value between observations (e.g. rms = 0.08 Å for $H\beta$) exceeds the formal error on each individual observation (typically 0.04 Å for $H\beta$). The source of excess scatter appears to be slight ripples in the relative continuum shapes between the observations. To account for the systematic error floor, we adopt the mean over the eight measurements and use the observed scatter to derive the error in the mean (0.03 Å for $H\beta$). The spectrum obtained for ESO325−G004 in the 6dF Galaxy Survey (Jones et al. 2004, 2009), in an aperture of radius 3.35 arcsec, yields index values compatible with the VIMOS measurements, but with uncertainties around six times larger.

We use the index data to derive constraints on the stellar mass-to-light ratio assuming an MW-like (Kroupa 2001) IMF. We denote this quantity as Υ_{MW}, while the true stellar mass-to-light ratio is M_*/L, and $\alpha_{MW} = (M_*/L)/\Upsilon_{MW}$ is the mass normalization factor' of the true IMF relative to Kroupa. In this convention, a Chabrier IMF has $\alpha_{MW} = 0.87$, a Salpeter IMF has $\alpha_{MW} = 1.55$, and a 'heavyweight' IMF as favoured by SLACS and CvD12b for massive ellipticals has $\alpha_{MW} = 2$.

To determine Υ_{MW}, we work in the context of models by Maraston (2005), Thomas, Maraston & Bender (2003) and Thomas, Maraston & Korn (2004), loosely referred to collectively as M05 hereafter. The M05 model set has the advantage of incorporating α-element enhancements in the index predictions (though not explicitly in the broad-band fluxes), as well as covering a comfortable range in super-solar total metallicity. We assume single-burst star-formation history models throughout the analysis. This simplification can be justified on the grounds that the galaxy shows no evidence for *recent* star formation, and that an extended star-formation history at *early* epochs is indistinguishable in terms of indices and colours from a single burst. Inspection of the 6dF red-arm spectrum does not show any evidence for emission at $H\alpha$, and hence there is no reason to suspect emission infilling contamination of the $H\beta$ and $H\gamma$ lines.

For a fixed IMF, the stellar mass-to-light ratio of a population depends mainly on age, and to a lesser extent on metallicity. Since individual line-strength indices depend on age, metallicity and abundance ratios (especially α/Fe), multiple indices are needed to constrain the age. We use $H\beta$ and $H\gamma_F$ as the primary age indicators, together with the α-element-dominated Mgb index and three iron-tracing indices (Fe5015, Fe5270, Fe5335). We compute the likelihood of the index data for all six features at each point in a grid spaced uniformly in log(age) [from log(5 Gyr) to log(12.5 Gyr)], total metallicity [Z/H] (from 0.1 to 0.4 dex) and $[\alpha/Fe]$ (from 0.1 to 0.5 dex). We determine the Υ_{MW} at each point in the age–metallicity grid using the EZGAL code of Mancone & Gonzalez (2012) to compute the mass-to-light ratio in the observed-frame $F814W$ band, in solar units, consistent with the convention used in our *HST* photometry. The M05 models assume no variation in Υ_{MW} with α/Fe, but this should be a small effect. For example, Percival et al. (2009) 'find that old α-enhanced ($[\alpha/Fe] = +0.4$) stellar population models are 2–3 per cent brighter in the I band than models with solar-scaled abundances at the same age and total metallicity.

Fig. 4 shows how the index data constrain the mass-to-light ratio. We derive the final probability distribution for Υ_{MW} by weighting the predictions according to their likelihoods (implicitly marginalizing over all the stellar population parameters), which yields $\Upsilon_{MW} = 3.01 \pm 0.14 \, (M/L)_{\odot, F814W}$. As a test of systematics within this method, we re-ran the analysis excluding each index in turn from the constraint set. As may be expected, the Balmer indices have the largest effect on the derived mass-to-light ratio. If $H\gamma_F$ is excluded, we obtain $\Upsilon_{MW} = 2.70 \pm 0.18 \, (M/L)_{\odot, F814W}$, while if $H\beta$ is excluded, we recover $\Upsilon_{MW} = 3.25^{+0.06}_{-0.11} \, (M/L)_{\odot, F814W}$. (The asymmetric errors arise from imposing a hard upper bound on the age, i.e. the galaxy is not permitted to be older than the Universe in the adopted cosmology.) Since these results differ by more than the error in the fit with both Balmer lines, we inflate the error to account for systematic uncertainties. The final estimated stellar
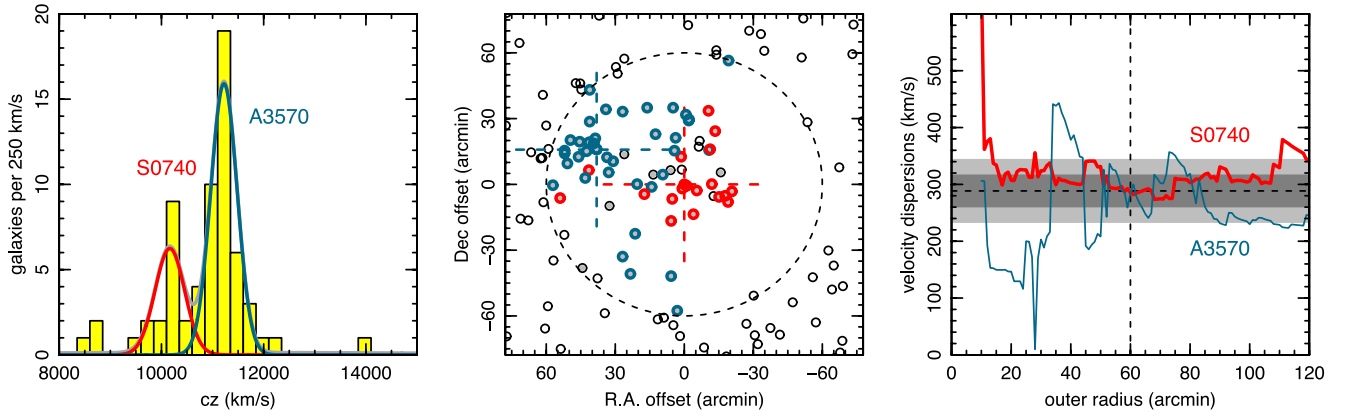
Figure 5. The velocity dispersion of Abell S0740. Left: histogram of velocity measurements from the NASA Extragalactic Database for galaxies within 60 arcmin of ESO325−G004. The curve shows the best-fitting Gaussian mixture model, highlighting the components for Abell S0740 (red) and Abell 3570 (blue). Centre: sky distribution of the galaxies with velocity measurements. For galaxies within 60 arcmin of ESO325−G004, membership assignments are indicated with the same colours as in the left-hand panel. The grey points with a black outline indicate the galaxies which were assigned to the smooth background. The unfilled symbols mark galaxies which were excluded before fitting. The assignment algorithm makes no use of the spatial information, but galaxies assigned to Abell S0740 and Abell 3570 are clearly centred near their respective dominant members (indicated by the cross-hairs). Right: the velocity dispersions of the two components derived from the Gaussian mixture model, as a function of the cut-off radius (the adopted value of 60 arcmin is marked by the vertical line). The 1σ and 2σ error regions for Abell S0740 are indicated by the dark and light grey bands, respectively.

population mass-to-light ratio, under the assumption of a Kroupa IMF, is $\Upsilon_{\rm MW} = 3.01 \pm 0.27$ $({\rm M/L})_{\odot, F814W}$. An equivalent analysis for the $F475W$ band yields $\Upsilon_{\rm MW} = 6.32 \pm 0.63$ $({\rm M/L})_{\odot, F475W}$.

To verify the robustness of our results, we have also applied a full-spectrum fitting method to the VIMOS data, using the CvD12a models. Within this model set, the spectra are best matched (and well matched) by models with the maximum age of 13.5 Gyr. Although the derived age is larger than that obtained from the M05 index-fitting approach, this is compensated by slightly smaller mass-to-light ratios at given age in CvD12a. In fact, the best-fitting model has $\Upsilon_{\rm MW} = 2.97$ $({\rm M/L})_{\odot, F814W}$ (after converting from Chabrier to Kroupa IMF, to match our convention). Hence, the results from the two approaches, using different models and different fitting methods, are indistinguishable.

We note also that assuming a single-burst population has little impact on the $\Upsilon_{\rm MW}$ derived for the $F814W$ band. To illustrate this, consider a two-burst star-formation history. The impact of the younger burst is *smaller* on $\Upsilon_{\rm MW}$ than on the age derived from the V band. Hence, for a *fixed* V-luminosity-weighted age (e.g. 9 Gyr), a two-burst model (e.g. 96 per cent 12 Gyr and 4 per cent 2 Gyr, by mass) has slightly *larger* $\Upsilon_{\rm MW}$ [3.25 $({\rm M/L})_{\odot, F814W}$] than a single burst [2.85 $({\rm M/L})_{\odot, F814W}$].

In summary, analysing the VIMOS spectrum confirms that the stellar population of ESO325−G004 is very old, and hence has a high mass-to-light ratio for a given IMF. Even for a Kroupa IMF, stars alone contribute a mass $\Upsilon_{\rm MW} L_{\rm Ein} = 1.2 \pm 0.1 \times 10^{11}$ $M_{\odot}$ within the Einstein radius, which is 80 ± 7 per cent of the total lensing mass.

3 DARK-MATTER CONTRIBUTION

The lensing mass refers to the total mass projected within the Einstein radius, including both stellar mass (living stars and remnants) and dark matter.[3] In this section, we use the statistics of halo profiles

in a cosmological *N*-body simulation to estimate the dark-matter correction and, crucially, the uncertainty in the correction.

To help constrain the dark-matter contribution in ESO325−G004, we use the velocity dispersion of its surrounding halo to select appropriate haloes from the simulation. The lens is the dominant member of a small galaxy group, catalogued Abell S0740 (Abell, Corwin & Olowin 1989), which is located close to another system, Abell 3570, at a projected distance of ∼40 arcmin and similar redshift. To measure the velocity dispersion of Abell S0740, we use the available (incomplete) redshift information compiled from the NASA Extragalactic Database.[4] Selecting galaxies within a radius of 60 arcmin and $|\Delta cz| < 5000$ km s^{-1} from ESO325−G004, we fit the redshift distribution using a Gaussian mixture model. The model includes two components representing Abell S0740 and Abell 3750, with mean redshift fixed to the velocities of their dominant galaxies (10 164 and 11 223 km s^{-1}, respectively), but fitting for the velocity dispersions. We allow an additional broad component to describe an approximately uniform background distribution. The best-fitting velocity dispersion for Abell S0740 under this model is $\sigma_v = 288 \pm 26$ km s^{-1} (the error is obtained by resampling using the posterior classification probabilities). We confirm the robustness of this measurement by re-fitting the model varying the outer cut-off radius, finding that σ_v is stable within the formal 2σ error range for cut-offs of 30–110 arcmin (see Fig. 5).

Neglecting (until Section 4) the possible contraction of the dark-matter halo in response to the dense baryonic component (Blumenthal et al. 1986), we can use dark-matter-only simulations to estimate the contribution of the halo to the projected mass inside the Einstein radius. We first select haloes from the Millennium

---

[3] In principle, there are also contributions from gas and from a central supermassive black hole. We assume that the gas mass projected within the

Einstein radius is negligible. This is equivalent to assuming that all gas is initially converted into stars, and that the gas lost in winds and supernovae is either recycled into further generations of stars or else expelled into a hot, low-density halo. Black hole mass contributions are small, as we show in Section 4.

[4] The majority of these redshifts are derived from the 6dF Galaxy Survey (Jones et al. 2004, 2009).
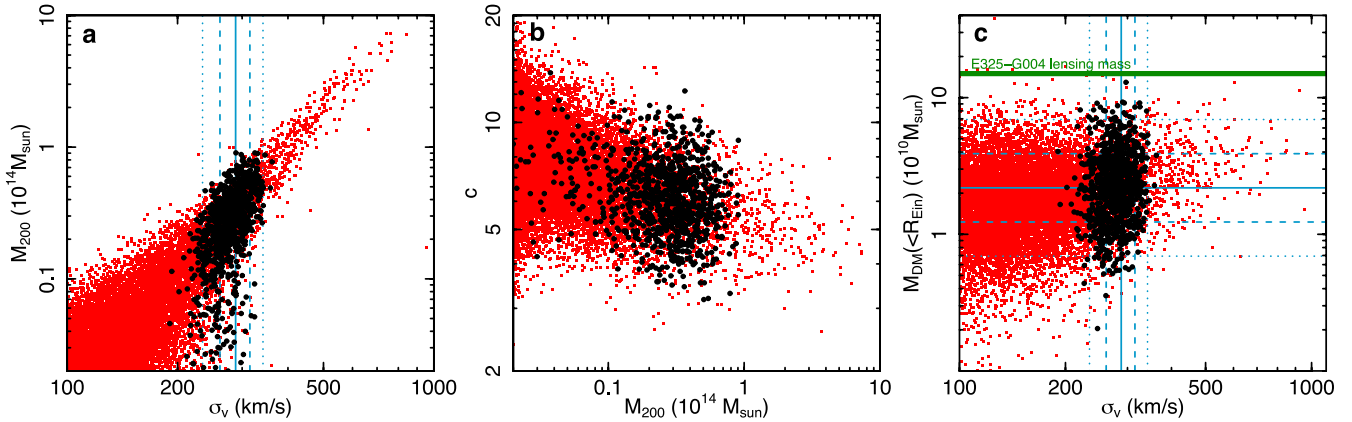
Figure 6. Constraints on the dark-matter contribution to the lensing mass derived from haloes in the Millennium Simulation. Left: the relationship between virial mass and velocity dispersion (the latter estimated from semi-analytic member galaxies, for an approximate match to the observational methods). The vertical bands show the measured velocity dispersion for Abell S0740 (the group which is dominated by ESO325−G004). The red points show a uniform sampling of all haloes, while the black points are sampled with a probability according to the measured velocity dispersion. Centre: the NFW concentration parameters assigned following the mass–concentration relation of Neto et al. (2007), as a function of the virial mass. Right: the dark-matter mass projected inside the Einstein radius, computed for an NFW profile with the assigned mass and concentration, as a function of the velocity dispersion. The horizontal lines show the median and 68 and 95 per cent intervals for enclosed dark-matter mass, which is well fitted by a Gaussian in $\log M_{\mathrm{DM}}$. The thick green line shows the total lensing mass M_{Ein}.

Simulation (Springel et al. 2005) having virial masses M_{200} greater than $10^{12}\,\mathrm{M}_\odot$ and compute their line-of-sight velocity dispersions based on member galaxies assigned in the semi-analytic model of De Lucia & Blaizot (2007). We then draw a large random sample from these haloes, with selection probability given by a Gaussian describing our constraint on σ_v for Abell S0740, i.e. with mean $288\,\mathrm{km\,s^{-1}}$ and standard deviation $26\,\mathrm{km\,s^{-1}}$. We represent each halo by an NFW profile (Navarro et al. 1996), with the concentration parameter, c, assigned according to the statistical distribution determined as a function of mass by Neto et al. (2007) for 'relaxed' haloes. We assume that at fixed halo mass, c is uncorrelated with the velocity dispersion, since the latter is obtained from all galaxies assigned to the halo, and hence is a large-aperture measurement. To compute M_{DM}, the dark-matter mass projected within the Einstein radius, for a given halo mass and concentration, we employ the analytic results presented by Łokas & Mamon (2001). The relationships between σ_v, M_{200}, c and M_{DM} are shown in Fig. 6. The derived distribution of dark halo contribution for the σ_v-matched sample can be accurately represented by a Gaussian in $\log (M_{\mathrm{DM}}/\mathrm{M}_\odot)$, with mean 10.34 and standard deviation 0.25. Perhaps surprisingly, the distribution of M_{DM} is only weakly dependent on velocity dispersion: although large σ_v is a predictor for higher halo mass, such haloes have lower concentration and hence a smaller fraction of their mass projected inside R_{Ein}.

Comparing this distribution to the lensing estimate, we find that dark matter contributes 15^{+11}_{-6} per cent of the total mass projected within R_{Ein}, in the absence of baryonic contraction effects. The estimated dark-matter component, added to the stellar mass from Section 2.3 (80 ± 7 per cent with a Kroupa IMF), is thus sufficient to reproduce the observed lensing configuration.

4   CONSTRAINTS ON THE IMF

The previous sections have presented measurements or estimates for the total lensing mass M_{Ein}, the dark-matter mass M_{DM}, the luminosity L_{F814W} and the stellar population model mass-to-light ratio assuming a Kroupa IMF (Υ_{MW}). All of these quantities refer

to mass and luminosity projected within the Einstein radius. Combining these inputs, the IMF mass normalization factor is simply

$$\alpha_{\mathrm{MW}} = \frac{M_{\mathrm{Ein}} - M_{\mathrm{DM}}}{L_{F814W}} \frac{1}{\Upsilon_{\mathrm{MW}}}.$$

In practice of course, each quantity above is described by a probability distribution, which can be approximated as lognormal for M_{DM} and normal for the other variables. Sampling from these distributions, we arrive at the probability distribution for α_{MW}, from which we determine whether various proposed IMFs are compatible with the observations for ESO325−G004. In this section, we first present the results using our preferred input parameters, and then explore the sensitivity of our result to various changes in the assumptions.

For the default result of this paper, we adopt the total mass $M_{\mathrm{Ein}} = 1.50 \pm 0.06 \times 10^{11}\,\mathrm{M}_\odot$ from lensing (including systematic errors), dark-matter mass $\log M_{\mathrm{DM}} = 10.34 \pm 0.25$ from halo statistics, luminosity $L_{F814W} = 4.07 \pm 0.08 \times 10^{10}\,\mathrm{L}_{\odot,\,F814W}$ from the *HST* photometry (including 2 per cent absolute calibration errors) and stellar population mass-to-light ratio for Kroupa IMF $\Upsilon_{\mathrm{MW}} = 3.01 \pm 0.27\,(\mathrm{M/L})_{\odot,\,F814W}$ from the VIMOS spectrum fit (including errors from index systematics). The adopted errors are conservative, including the various sources of systematic error assessed in earlier sections. Other possible systematics are probed using robustness tests below. With these inputs, the probability distribution for α_{MW} is as shown in Fig. 7 (thick black curve) and summarized in line 1 of Table 2. The distribution is fairly symmetric in α_{MW}, peaking at $\alpha_{\mathrm{MW}} = 1.04$, with a 68 per cent interval of ± 0.15. Hence, the results are consistent with an MW-like IMF, with either the Kroupa or the Chabrier form. A Salpeter or heavier IMF is disfavoured at the 99.8 per cent confidence level,[5] while a heavyweight IMF with $\alpha_{\mathrm{MW}} \geq 2$ is excluded with high significance.

---

[5] Note this is a one-tailed confidence limit, i.e. for a Gaussian distribution 84.1 per cent would correspond to a $+1\sigma$ deviation, and 99.8 per cent would correspond to $+2.9\sigma$. In practice, the distribution is not quite Gaussian, so we quote the probabilities estimated directly from the high-α_{MW} tail.
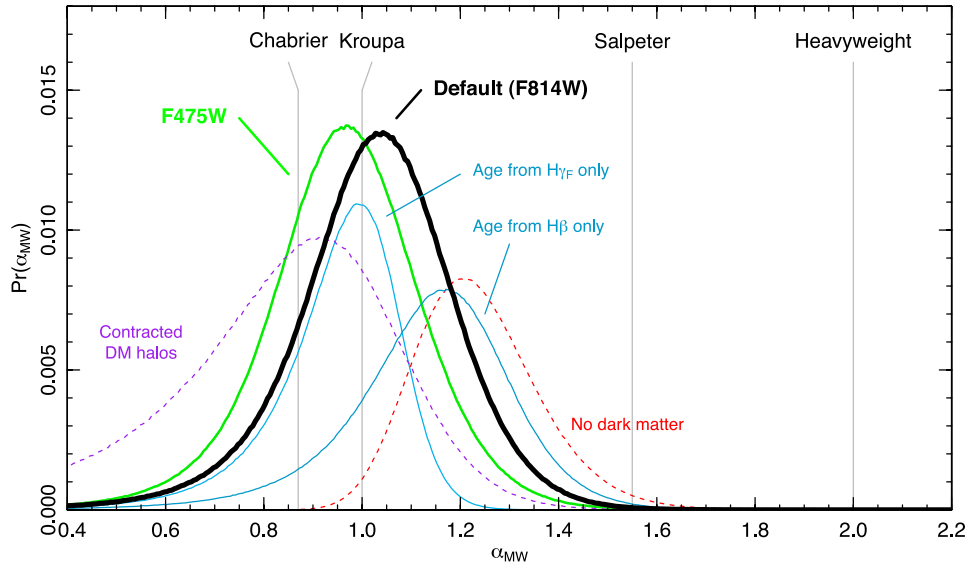
Figure 7. Probability distribution function for the IMF mass normalization factor α_{MW}, marginalizing over age and metallicity, and the contribution from dark matter. The thick black curve shows our default solution, while other curves indicate the effect of variations in the modelling. The green curve shows the results derived using the $F475W$ data. The blue curves illustrate the effect of using only one Balmer index ($H\beta$ or $H\gamma_F$) in the fit. The red dashed line results from setting the dark-matter contribution to zero, while for the purple curve, all dark-matter contributions are doubled to indicate the maximum likely halo contraction effect. Input parameters, best-fitting α_{MW} and the IMF probabilities associated with these curves are summarized in Table 2. The mass normalizations equivalent to IMFs are indicated. The 'heavyweight' line has $\alpha_{MW} = 2$, corresponding to the average for $\sigma > 300\,\mathrm{km\,s^{-1}}$ ellipticals, as derived by T10 and CvD12b.

An equivalent calculation for the $F475W$ band using $\Upsilon_{MW} = 6.32 \pm 0.63\,(\mathrm{M/L})_{\odot,\,F475W}$ and the $F475W$ luminosity of $2.07 \pm 0.04 \times 10^{10}\,\mathrm{L}_{\odot}$ yields $\alpha_{MW} = 0.97 \pm 0.15$, consistent with the default result (thick green curve in Fig. 7 and line 2 of Table 2). This agreement simply confirms that the best-fitting stellar population model correctly predicts the observed $F475W-F814W$ colour within R_{Ein}.

We have seen that the choice of Balmer indices in the stellar population fitting has the largest impact on the derived Υ_{MW}. This propagates trivially to the results for α_{MW} (blue curves in Fig. 7 and lines 3 and 4 of Table 2). If only $H\beta$ is used for age constraints, the best α_{MW} shifts upwards to 1.17, and the confidence with which a heavier-than-Salpeter IMF is excluded is reduced to 99.4 per cent. The heavyweight IMF remains firmly rejected. Allowing for α-enhanced model populations being slightly brighter than solar-scaled abundance models (Percival et al. 2009), the derived α_{MW} would be increased by ~2 per cent.

Our treatment of the dark-matter contribution incorporates the expected intrinsic scatter among haloes, under the assumption of pure dark-matter clustering. In practice, the halo of ESO325−G004 may deviate from the assumptions of this model, especially in the innermost regions, where the dark-matter distribution may contract in response to the dominant baryonic component. Simulations by different groups differ in their estimates of the strength of this effect (e.g. see the discussion in Gnedin et al. 2011). Reviewing comparisons of hydrodynamic simulations against dissipationless control simulations, we note the following: Gnedin et al. (2011) find enhancements in the inner dark-matter mass (enclosed within 1 per cent of the halo virial radius) by factors of 2–4. Johansson, Naab & Ostriker (2012) find that the central dark-matter mass (enclosed within 2 kpc) is enhanced by a factor of 2.3 (their halo A2). Remus et al. (2013) found central dark-matter density enhanced by a factor of 2–3 (their fig. 1). These results are generally for galaxy-scale haloes. For $10^{13}\,\mathrm{M}_{\odot}$ groups (more relevant to ESO325−G004/Abell S0740),

Table 2. Summary of constraints obtained for the IMF mass normalization parameter α_{MW} in ESO325−G004. The six lines correspond to the curves shown in Fig. 7. Υ_{MW} is the mass-to-light ratio of the best-fitting stellar population model, assuming a Kroupa IMF, L_{Ein} is the luminosity inside the Einstein radius R_{Ein} and M_{DM} is the estimated dark-matter mass projected inside R_{Ein}. Probabilities estimated from the distributions for α_{MW} are $\mathrm{Pr}(\alpha_{MW} < 1)$, the probability that the IMF mass normalization is smaller than Kroupa; $\mathrm{Pr}(\alpha_{MW} > 1.55)$, the probability that the IMF is heavier than Salpeter; and $\mathrm{Pr}(\alpha_{MW} > 2)$, the probability that the IMF normalization is larger than 2.0, which is the mean α_{MW} derived for $\sigma > 300\,\mathrm{km\,s^{-1}}$ ellipticals by T10 and CvD12b.

No.		$\Upsilon_{MW}/(\mathrm{M/L})_{\odot}$	$L_{Ein}/10^{10}\mathrm{L}_{\odot}$	$\log M_{DM}/\mathrm{M}_{\odot}$	α_{MW}	$\mathrm{Pr}(\alpha_{MW} < 1)$	$\mathrm{Pr}(\alpha_{MW} > 1.55)$	$\mathrm{Pr}(\alpha_{MW} > 2)$
(1)	Default	3.01 ± 0.27	4.07 ± 0.08	10.34 ± 0.25	$1.04^{+0.15}_{-0.15}$	0.354 686	0.001 545	0.000 002
(2)	$F475W$ band	6.32 ± 0.63	2.07 ± 0.04	10.34 ± 0.25	$0.97^{+0.15}_{-0.15}$	0.531 162	0.000 873	0.000 002
(3)	$H\gamma_F$ only	$3.25^{+0.06}_{-0.11}$	4.07 ± 0.08	10.34 ± 0.25	$0.99^{+0.09}_{-0.11}$	0.577 770	<0.000 001	<0.000 001
(4)	$H\beta$ only	2.70 ± 0.18	4.07 ± 0.08	10.34 ± 0.25	$1.17^{+0.13}_{-0.15}$	0.138 487	0.006 241	<0.000 001
(5)	Contracted haloes	3.01 ± 0.27	4.07 ± 0.08	10.64 ± 0.25	$0.91^{+0.17}_{-0.21}$	0.680 350	0.000 332	<0.000 001
(6)	No dark matter	3.01 ± 0.27	4.07 ± 0.08	–	$1.20^{+0.13}_{-0.11}$	0.012 379	0.019 302	0.000 030

Duffy et al. (2010) find smaller enhancements, between zero and 50 per cent in the inner dark-matter density, depending on the adopted feedback prescription. All of these factors refer to three-dimensional densities or enclosed masses, rather than projected quantities. On balance, we adopt a factor of 2 as an upper limit to the likely effect of halo contraction. Rescaling our input distribution of M_{DM} by this factor, we would recover $\alpha_{MW} = 0.91^{+0.17}_{-0.21}$ (purple dashed curve in Fig. 7 and line 5 of Table 2). An alternative limiting case is to assume that dark matter is negligible within the Einstein radius, so that stars must account for the entirety of the lensing mass (red dashed curve in Fig. 7 and line 4 of Table 2). Under this extreme model, the best α_{MW} is $1.20^{+0.13}_{-0.11}$, which is marginally consistent with a heavier-than-Salpeter IMF (98 per cent), but still incompatible with the heavyweight models.

We neglected the extra mass that would be contributed by a central supermassive black hole. From the M_{BH}-σ relationship given by McConnell et al. (2011) for early-type galaxies, the mean expected black hole mass is 2.5×10^9 M$_\odot$, or 2 per cent of M_{Ein}. If we account also for the intrinsic scatter of 0.38 dex around the McConnell et al. M_{BH}-σ relation, the derived α_{MW} would be slightly reduced, relative to our default solution, to 1.01 ± 0.15.

For the default result, we used the M05 stellar population models because these provide the most convenient predictions for both mass-to-light ratios and line-strength indices in metal-rich, α-enhanced populations. We have already noted that a full-spectrum fitting approach, using the CvD12a models, yields essentially identical Υ_{MW}, and consequently the same result for α_{MW}. To test the effect of using other model sets, we discard all information from the line-strength indices, and instead impose an external prior for the age. Given the mass of the galaxy, its pure absorption spectrum including the absence of any emission at Hα (from the 6dF spectrum) and smooth light distribution (even in the central regions, where dust features and star-forming rings are sometimes seen in *HST* observations of ellipticals – e.g. Laine et al. 2003; Martel et al. 2004), it is unlikely that ESO325−G004 has experienced substantial star formation since $z < 1$. We adopt a Gaussian prior on (*I*-band luminosity-weighted) formation redshift with mean 2.5 and standard deviation 0.75. Combining this with the M05 predictions, using EZGAL, for 1.5 times solar metallicity (the maximum implemented for all model sets), we obtain a predicted stellar mass-to-light ratio $\Upsilon = 2.67^{+0.15}_{-0.25}$ (M/L)$_{\odot, F814W}$. This is slightly smaller than our spectroscopic estimate, since the spectroscopy favours earlier formation and higher metallicity. Combining this estimate with lensing and the dark-matter contributions would yield $\alpha_{MW} = 1.18^{+0.16}_{-0.17}$. We can now derive equivalent estimates for other stellar population models, using the same external age prior, and compare to this baseline value. The results for α_{MW} are 0.96 for Bruzual & Charlot (2003),[6] 1.10 for Conroy, Gunn & White (2009), 1.05 for Percival et al. (2009) and 1.12 for Fioc & Rocca-Volmerange (1997), all with uncertainties of ∼0.15. In all cases, the models are as implemented by default in EZGAL (see Mancone & Gonzalez 2012), with the maximum 1.5 times solar metallicity. Hence, for common assumptions on the galaxy age, other stellar population models yield *smaller* IMF normalizations than M05, by up to 20 per cent.[7] We conclude that the derived IMF constraint is fairly insensitive to the choice of stellar population models among the currently favoured sets.

Finally, we note that rescaling the distance assumed for ESO325−G004 affects α_{MW} linearly. If instead of placing the galaxy at its Hubble-flow distance, we assign it the same distance as Abell 3570, then α_{MW} is increased to 1.15. If instead we allow the galaxy a large positive peculiar velocity[8] of 1000 km s^{-1}, then α_{MW} is reduced to 0.95.

To summarize, using a combination of lensing and stellar population constraints, with correction for dark-matter contributions based on simulations, we find that ESO325−G004 has a stellar mass-to-light ratio compatible with an MW-like (Kroupa or Chabrier) IMF. A Salpeter IMF is significantly disfavoured, and a heavyweight IMF is excluded. The statistical errors in the IMF mass normalization factor are ∼15 per cent; a range of robustness tests suggest that systematic errors are also 10–15 per cent. The most relevant measured and derived parameters for the ESO325−G004 system are provided in Table 3 for reference.

5 DISCUSSION

In this section, we examine how the results obtained for ESO325−G004 compare to recent results which favour heavier IMFs in ellipticals with similar properties. We focus in particular on the apparent disagreement between our results and those of T10 and CvD12b, and speculate on potential explanations for this tension.

5.1 Comparison to SLACS lensing results

As described in Section 1, SLACS is a spectroscopically defined lens sample based on SDSS. Lens systems were identified from the presence of discordant emission lines in the spectra. For the main study, an *HST* follow-up was obtained for systems with at least two lines, in practice usually [O II] 3727 Å and Hβ or [O III] 5007 Å. A few additional targets with strong [O II] detections, but no corroborating lines, were also followed up.

Fig. 8 (upper panel) compares our result for ESO325−G004 against the correlation of α_{MW} with velocity dispersion (σ) from SLACS, among other works. We have increased the velocity dispersions from T10 by 7 per cent, as an aperture correction to $R_{eff}/8$ (this aperture is selected for consistency with CvD12b in the same figure, discussed below). Apart from this correction, and conversion to our definition of α_{MW}, the points are the same as in fig. 4 of T10. As reported by T10, the SLACS lenses follow a clear trend of increasing IMF mass normalization with increasing σ, reaching $\alpha \approx 2$ at $\sigma > 300$ km s^{-1}. As they also note, the observed scatter is compatible with *no* intrinsic dispersion around the α_{MW}-σ relation. The 12 galaxies with $\sigma > 300$ km s^{-1} (after aperture correction to $R_{eff}/8$ as in Fig. 8) have a mean α_{MW} of 2.04 and a χ^2 of only 2.3 around this mean [Pr($\chi^2_{\nu=11} \leq 2.3$) = 0.003]. At face value, then, our measurement of $\alpha_{MW} = 1.04 \pm 0.15$ for ESO325−G004, a galaxy with a similar velocity dispersion, is not only significantly different from the *mean* SLACS α_{MW}, but is also inconsistent with the *distribution* of α_{MW} from SLACS at comparable velocity dispersion. The small lensing mass of ESO325−G004 shows, at the very least, that not all $\sigma > 300$ km s^{-1} ellipticals have heavyweight IMFs, contrary to the implications of T10.

---

[6] Unchanged if we use instead the unpublished 2007 update to these models.
[7] It should not be assumed that identical shifts would apply to the *full* analysis including spectroscopy, since the other models may predict slightly different index strengths as well as different mass-to-light ratios.

[8] ESO325−G004 lies in the foreground of the Shapley supercluster; the original ACS data were obtained as part of an effort to measure peculiar velocities in this region.

Table 3. Summary of relevant parameters of the ESO325−G004 lens system.

Quantity	Symbol	Value	Comments
Lens redshift (heliocentric)		0.0339	From 6dF
Lens redshift (CMB frame)	z_l	0.0347	
Lens angular-diameter distance	D_l	142 Mpc	From z_l with *WMAP*7 cosmology
Angular scale at lens		0.687 kpc arcsec^{-1}	From D_l
Lens half-light radius	$R_{\rm Eff}$	12.3 arcsec	From the ACS *F814W* image
Lens stellar velocity dispersion	σ	331 ± 2 km s^{-1}	$R_{\rm eff}/8$ aperture
Lens luminosity distance		152 Mpc	From z_l with *WMAP*7 cosmology
Lens distance modulus		35.909	
Source redshift	z_s	2.141	From X-SHOOTER
Lensing geometry factor	$f_z = D_s/D_{ls}$	1.027	From z_l and z_s with *WMAP*7 cosmology
Lensing critical surface density	$\Sigma_{\rm crit}$	5.70×10^9 M$_\odot$ arcsec^{-2}	From f_z and D_l
Einstein radius	$R_{\rm Ein}$	2.85 arcsec	SIS mass model (S05)
Luminosity inside the Einstein radius	L_{F814W}	$4.07 \pm 0.08 \times 10^{10}$ L$_{\odot, F814W}$	ACS photometry, corrected for extinction
Total lensing mass-to-light ratio	$M_{\rm MFL}/L_{F814W}$	3.69 ± 0.03(M/L)$_{\odot, F814W}$	From the MFL model
Total lensing mass inside $R_{\rm Ein}$	$M_{\rm Ein}^{\rm MFL}$	$1.50 \pm 0.06 \times 10^{11}$ M$_\odot$	From the MFL model
S0740 group velocity dispersion	σ_v	288 ± 26 km s^{-1}	Literature redshifts; decomposed from Abell 3570
Dark-matter mass within $R_{\rm Ein}$	$M_{\rm DM}$	$2.19^{+1.70}_{-0.96} \times 10^{10}$ M$_\odot$	From Millennium Simulation halo statistics
Stellar mass inside $R_{\rm Ein}$	M_*	$1.28^{+0.10}_{-0.17} \times 10^{11}$ M$_\odot$	From $M_{\rm Ein}^{\rm MFL}$ and $M_{\rm DM}$
Stellar mass-to-light ratio	M_*/L_{F814W}	$3.14^{+0.24}_{-0.42}$(M/L)$_{\odot, F814W}$	From M_* and L_{F814W}
Stellar mass-to-light ratio for Kroupa IMF	$\Upsilon_{\rm MW}$	3.01 ± 0.25 (M/L)$_{\odot, F814W}$	From fit to VIMOS line-strength indices
IMF mass factor relative to Kroupa	$\alpha_{\rm MW}$	1.04 ± 0.15	M_*/L_{F814W} and $\Upsilon_{\rm MW}$

The SLACS analysis method differs in several ways from our approach, for example using only colour information to derive the age and metallicity, rather than high-S/N spectroscopy, and fitting a halo model directly to each lens using the measured velocity dispersion of the galaxy, instead of using simulation statistics. Additionally, the lensing geometry of ESO325−G004 is quite atypical of the average properties of SLACS sample lenses, due to differences in selection/discovery methods.

The ESO325−G004 lens system differs from SLACS systems in both the redshift of the lens and that of the source. The redshift of ESO325−G004 is smaller than that of any SLACS lens and a factor of 7.5 smaller than the median for the $\sigma > 300$ km s^{-1} SLACS lenses. Assuming only that dark matter follows a more extended profile than the stellar mass, it follows that the dark-matter fraction within the Einstein radius is an increasing function of the ratio $R_{\rm Ein}/R_{\rm eff}$. For ESO325−G004, this ratio is 0.23, compared to a median of 0.62 for the twelve $\sigma > 300$ km s^{-1} SLACS lenses (Auger et al. 2009). Hence, in ESO325−G004, the dark-matter contribution is smaller, and all of the systematic and random uncertainties in modelling the dark matter are suppressed.[9]

At $z_s = 2.141$, the redshift of the source in ESO325−G004 is much larger than that in any SLACS system. The absence of high-redshift sources in SLACS is a simple consequence of the spectroscopic selection method: for $z_s > 0.8$–0.9, the Hβ and [O III] lines shift out of the SDSS spectral range; the single-line [O II] objects provide a few higher redshift lenses, but there are none at $z_s > 1.1$ For a given lens redshift and Einstein radius, a closer source implies a more massive lens galaxy, so the SLACS selection of low-redshift source galaxies potentially biases their sample towards lenses with large central (stellar plus dark-matter) masses. This effect could be the cause of the significant ($\sim 3\sigma$) anticorrelation between $\alpha_{\rm MW}$

and source redshift in the SLACS sample (Fig. 9). For the twelve $\sigma > 300$ km s^{-1} SLACS lenses, the mean source redshift is 0.52 and the mean lens redshift is 0.26. If we assume that $\sigma > 300$ km s^{-1} galaxies actually span a wide range in $\alpha_{\rm MW}$, we can ask which values correspond to source redshifts that are detectable in SDSS. Computing the geometric factor for $z_l = 0.26$ and a range of z_s, we find that the source-redshift selection limit of $z < 0.85$ (for multiple-line source detection) imposes a limit of $\alpha_{\rm MW} > 1.5$ for these galaxies. Sources at $z \gtrsim 2$ would correspond to $\alpha_{\rm MW} \approx 1.2$, but are undiscoverable with the SLACS approach. Hence, SLACS might be selecting only the highest $\alpha_{\rm MW}$ galaxies within a broad intrinsic distribution. A counter-argument to this suggestion is that Auger et al. (2010) find the SLACS lens galaxies to follow the same Fundamental Plane correlations as derived for general SDSS samples, which would appear to argue against such a bias, unless the distribution *within* the plane was unrepresentative. A full investigation of source-redshift selection bias is beyond the scope of the present paper, but could likely be carried out by generalizing the methods of Arneson, Brownstein & Bolton (2012).

By contrast, our serendipitous morphological discovery of arcs behind ESO325−G004, and subsequent spectroscopy to secure the source redshift, is free from this 'source-redshift' bias. Hence, if there is a very broad intrinsic distribution of $\alpha_{\rm MW}$ (or alternatively, a distribution of deviations from the assumed dark-matter halo properties), SLACS may select only those galaxies at the massive extreme, while ESO325−G004 provides a single but more representative sample from the distribution. In this context, we note that Spiniello et al. (2011), analysing a morphologically identified $\sigma \approx 340$ km s^{-1} lens with $z_s = 2.38$ (Belokurov et al. 2007), rule out very heavy IMFs, while MW-like or Salpeter distributions are compatible with lensing and dynamical constraints. This result broadly supports our suggestion that different methods of selecting lenses may lead to different distributions for the recovered $\alpha_{\rm MW}$; a further follow-up of large morphologically defined lens samples is required to test this possibility.

[9] Note that T10 report average dark-matter fractions of only ~ 20 per cent, but this is contingent upon a particular (spherical uncontracted NFW) model for the haloes.
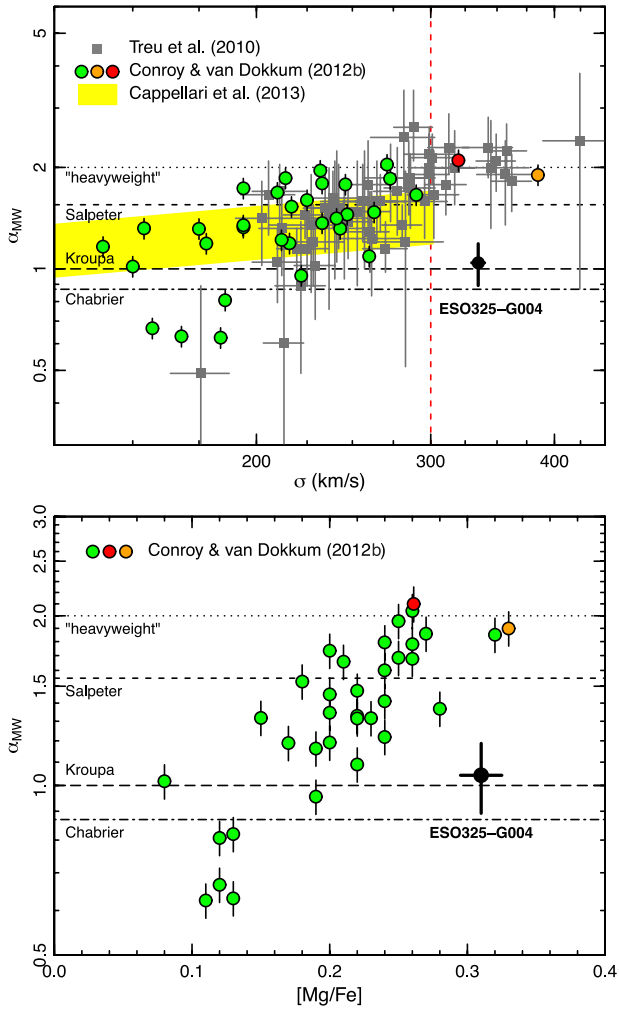
Figure 8. Upper panel: result for ESO325−G004 compared to the α_{MW}-σ relations from the SLACS lenses (T10), spectroscopic analysis (CvD12b) and stellar dynamics (Cappellari et al. 2013). We highlight the $\sigma > 300\,\mathrm{km\,s^{-1}}$ regime probed by ESO325−G004, in which both T10 and CvD12b favour heavyweight IMFs on average. Lower panel: equivalent comparison for the α_{MW}–[Mg/Fe] relation from CvD12b. The vertical axis scale is not identical to the upper panel. Velocity and [Mg/Fe] are as measured within an aperture of $R_{eff}/8$ for ESO325−G004 and CvD12b, and corrected to this aperture for T10 and Cappellari et al. (2013). In both panels, the red point represents a stacked spectrum of four massive ellipticals in Virgo from van Dokkum & Conroy (2010). The orange point denotes M87.

5.2 Comparison to the CvD dwarf-star-indicator method

The spectroscopic method used by CvD12b is not sensitive explicitly to mass, but instead to the characteristic features of dwarf stars in the integrated spectra of galaxies. The implications for α_{MW} are derived assuming a three-part power-law IMF, fixed to the Salpeter slope at $M > M_\odot$ but allowed to vary to steeper or shallower slopes at lower mass. CvD12b find an increasing trend of α_{MW} as a function of velocity dispersion, and also as a function of the Mg/Fe abundance ratio.[10] The CvD12b sample has few galaxies at the high velocity dispersions and Mg/Fe ratios similar to ESO325−G004. At

---

[10] These two properties are correlated. A fit for α_{MW} versus both σ and [Mg/Fe] suggests that the latter is dominant in driving the relationship.
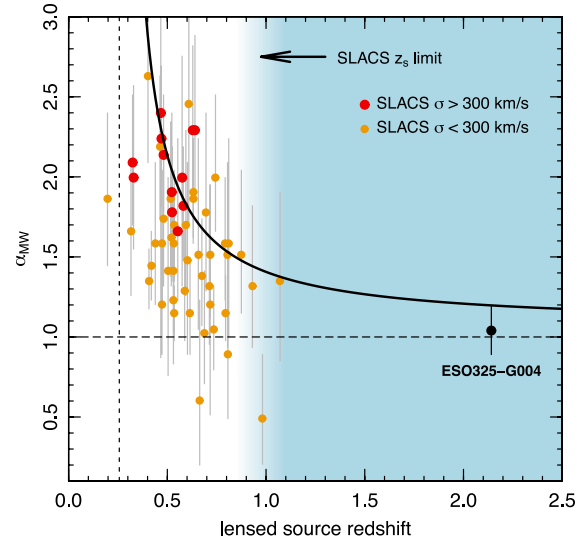

Figure 9. Derived α_{MW} versus source galaxy redshift for SLACS and for ESO325−G004. The red points highlight the most massive SLACS lenses ($\sigma > 300\,\mathrm{km\,s^{-1}}$). The black curve shows the relationship between α_{MW} and source redshift through the lensing geometry factor ($f_z = D_s/D_{ls}$), computed for the median lens redshift $\langle z_l \rangle = 0.26$ of the massive SLACS galaxies (shown as the vertical dashed line) and normalized to $\langle \alpha_{MW} \rangle = 2.04$ found for these galaxies. The curve indicates the implied α_{MW} if these galaxies were lensing sources at other redshifts. The source-redshift limit imposed by the SDSS spectroscopic selection translates to a limit of $\alpha_{MW} \gtrsim 1.5$ for the high-σ SLACS lenses. Note that the curve depends on z_{lens}. The lower-σ SLACS systems (orange) have smaller z_{lens} on average, so these galaxies can lens low-redshift sources even for $\alpha_{MW} \lesssim 1.5$.

$\sigma > 300\,\mathrm{km\,s^{-1}}$, the sample contains only M87 and a stacked spectrum of four Virgo cluster galaxies from the original van Dokkum & Conroy (2010) study. These spectra both yield $\alpha_{MW} \approx 2$, in agreement with the SLACS results at similar velocity dispersion. La Barbera et al. (2013) have analysed dwarf-sensitive features in a stacked sample of early-type galaxies from SDSS, assuming single or broken power-law IMFs. As in CvD12b, there is a strong trend of α_{MW} with velocity dispersion. At $\sigma \approx 300\,\mathrm{km\,s^{-1}}$, the best-fitting broken power-law IMF models have $\alpha_{MW} \approx 1.7$, similar to the CvD12b results at similar σ. Spiniello et al. (2013), using a different set of spectral features, recover a weaker dependence of the IMF slope on σ, with slopes only mildly steeper than Salpeter at $\sigma \approx 300\,\mathrm{km\,s^{-1}}$.

Fig. 8 compares ESO325−G004 with the CvD12b trends in both the α_{MW}−σ and the α_{MW}–[Mg/Fe] relations. For consistency with CvD12b in placing ESO325−G004 on the horizontal axis of the figures, we use the velocity dispersion and [Mg/Fe] ratio measured from a spectrum extracted from the VIMOS data within a radius of $R_{eff}/8$. The abundance ratio is derived using full-spectrum fitting to the CvD12a models, allowing for variation in other relevant parameters (age, Fe/H, C/Fe). This analysis yields [Mg/Fe] = 0.31 ± 0.02 and $\sigma = 331 \pm 2\,\mathrm{km\,s^{-1}}$, where errors are derived from repeatability over the separate VIMOS exposures.

The lensing-derived α_{MW} for ESO325−G004 is inconsistent with the *average* α_{MW} from CvD12b, for galaxies of similar properties. However, the intrinsic scatter at high σ is poorly determined, so this discrepancy could simply indicate that ESO325−G004 has a lighter-than-average IMF within a broad underlying distribution. In
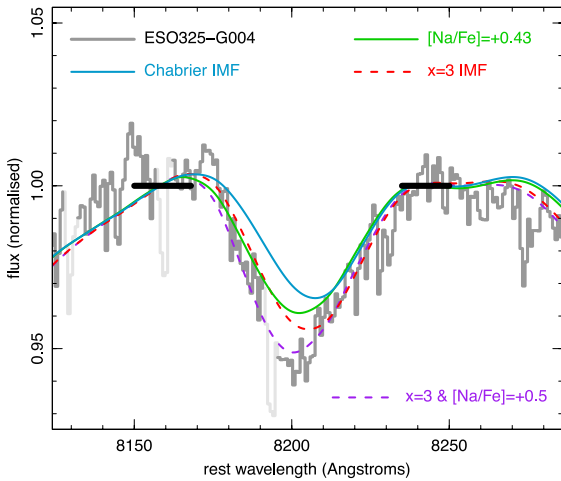
Figure 10. The dwarf-sensitive Na I feature in ESO325−G004, compared to models from CvD12a. The light grey sections indicate pixels affected by strong sky lines. All models shown have [α/Fe] = +0.3 and age 13.5 Gyr. The spectra are normalized at the continuum regions of the index defined by Spiniello et al. (2012), shown as black bars. The blue and green curves denote Chabrier IMF models with solar and enhanced sodium abundances, respectively. [Na/Fe] = +0.43 is the average obtained for $\sigma \approx 300\,\mathrm{km\,s^{-1}}$ galaxies in SDSS by Conroy, Graves & van Dokkum (2013a). A bottom-heavy IMF model, with $x = 3$ (in the convention where the Salpeter slope is 2.3) is shown in red. Matching the observed spectrum requires both $x = 3$ *and* enhancement of sodium (purple line). The $x = 3$ IMF models would have $\alpha_{\mathrm{MW}} > 2$, and hence would violate the lensing limits.

this scenario, we would expect that this galaxy would also exhibit weaker dwarf-star signatures than average for massive galaxies.

To test this possibility, we have obtained a far-red spectrum of ESO325−G004 to measure the Na I feature and hence compare dwarf-star indicators versus lensing constraints directly. We observed ESO325−G004 with FORS2 (Appenzeller et al. 1998) at UT1 of the VLT, on 2013 May 10. The observations were made using the 1028z grism, with a 1.3 arcsec slit width, providing a wavelength coverage of 7730–9500 Å, with a 2.5 Å FWHM resolution, sampled at 0.8 Å pixel^{-1}. The total exposure time was 1570 s. To mimic a circular aperture measurement sampling the light within R_{Ein}, we extracted the spectrum within ±2.85 arcsec from the galaxy centre, weighted linearly with distance. Fig. 10 shows the Na I region in the resulting spectrum (which has S/N ≈ 150 Å^{-1}), in comparison with models from CvD12a.[11] The strength of Na I in ESO325−G004 appears to be similar to that in other high-σ elliptical galaxies (Conroy & van Dokkum 2012b; van Dokkum & Conroy 2010; Ferreras et al. 2013). The observed absorption is much stronger than that in the models with MW-like IMF, even allowing for enhancement of sodium abundances by 0.43 dex (the average for $\sigma \approx 300\,\mathrm{km\,s^{-1}}$ found by Conroy et al. 2013a). To reproduce the observed Na I feature in the CvD12a models would require either a substantially steeper IMF (e.g. a single power law with slope $x \gtrsim 3$ in the convention where Salpeter has $x = 2.35$) or a larger enhancement in sodium, or some combination of these effects. For the Chabrier IMF, which is consistent with the lensing constraint, the sodium enhancement would have to be quite extreme, e.g. [Na/Fe] ≈ +1.2, which is not supported by the strength of the Na D absorption in the VIMOS spectrum..

Although a single power law with $x \gtrsim 3$ would certainly violate the lensing-mass constraint, it is conceivable that a more flexible IMF prescription as used by CvD12b would be able to reproduce the observed Na I without requiring excessive mass contributions from low-mass stars. If so, it may be possible to use the lensing mass in combination with the spectroscopic signatures to probe the detailed shape of the IMF. For example, La Barbera et al. (2013) have shown a comparison of M_*/L derived from dwarf-star indicators (including Na I) against dynamical estimates, which excludes single power laws, but yields consistent results when two-part broken power-law IMFs are adopted. ESO325−G004 provides an opportunity to conduct a similar test for an individual galaxy using a robust external mass estimate.[12]

In summary, our lensing measurement of α_{MW} for ESO325−G004 is inconsistent with the average derived from CvD12b for galaxies of similar properties. While it is possible that ESO325−G004 is an outlier from a distribution of α_{MW}, the strong measured Na I absorption does not support this interpretation, unless the sodium abundance is much larger than average for $\sigma \approx 300\,\mathrm{km\,s^{-1}}$ ellipticals. The Na I measurement suggests some tension between the lensing mass and the IMF-sensitive spectral features for this galaxy, but further work is required before a firm conclusion can be drawn.

5.3 Comparison to stellar dynamics

We comment here briefly on a comparison to recent dynamical estimates of M_*/L in early-type galaxy samples, and make a dynamical estimate for the mass of ESO325−G004.

The upper panel of Fig. 8 includes the estimated α_{MW}-σ relation from Cappellari et al. (2013) derived from the Atlas3D survey (from their fig. 13, upper panel). The velocity dispersions have been increased by 10 per cent as an approximate aperture correction to $R_{\mathrm{eff}}/8$ in common with the other data sources plotted. Cappellari et al. recover a much shallower α_{MW}-σ relation than T10, but it should be noted that Atlas3D and SLACS overlap only for $\sigma = 200$–$300\,\mathrm{km\,s^{-1}}$, and in this interval the agreement is fairly close. ESO325−G004 does not lie within the σ range probed by Atlas3D. Extrapolation of the Cappellari et al. trend would suggest a Salpeter-like $\alpha_{\mathrm{MW}} \approx 1.5$. Allowing also for the possible intrinsic scatter (estimated as 20 per cent at lower σ), ESO325−G004 is marginally consistent with the Cappellari et al. trend.

A smaller dynamical study of ellipticals in the Coma and Abell 262 clusters (Thomas et al. 2011; Wegner et al. 2012) finds a trend which appears more similar to the SLACS trend, with average $\alpha_{\mathrm{MW}} \approx 2$ for the five Coma galaxies with $\sigma > 300\,\mathrm{km\,s^{-1}}$ (after aperture correction to $R_{\mathrm{eff}}/8$).

We can make a crude estimate of the dynamical mass of ESO325−G004 using the virial mass estimator, $M_{\mathrm{dyn}} = 5\sigma_{\mathrm{Eff}}^2 R_{\mathrm{Eff}}/G$, where σ_{Eff} is the velocity dispersion estimated within the effective radius. Using the measured half-light radius of 8.5 kpc and $\sigma_{\mathrm{Eff}} = 310\,\mathrm{km\,s^{-1}}$ (allowing for an 8 per cent aperture correction from R_{Ein} to R_{Eff}), this estimator yields $M_{\mathrm{dyn}} = 9.4 \pm 1.3 \times 10^{11}\,\mathrm{M_\odot}$. The error is derived from the galaxy-to-galaxy scatter of 14 per cent found by Cappellari et al. (2006) through comparison to masses derived from Schwarzschild models. This quantity should represent the total mass extrapolated to large

---

[11] Strictly, the models shown are updated versions, with improved abundance response functions.

[12] While this paper was under review, Barnabè et al. (2013) published an analysis along these lines, constraining the slope and low-mass cut-off for a power-law IMF in two SLACS lenses.

radius. From the luminosity profile, we find that 18 per cent of the total flux is projected inside the Einstein radius, so for a constant mass-to-light ratio, the *dynamical* estimate of $M_{\rm Ein}$ is $1.7 \pm 0.2 \times 10^{11}\,M_{\odot}$, which is consistent with the lensing estimate. Note that $M_{\rm Ein}$ from lensing is a much more direct and robust measurement of the mass enclosed within a small aperture, where dark-matter contributions are small and the stellar populations well determined. The value of $\alpha_{\rm MW}$ from lensing should thus be more reliable and accurate than dynamical estimates.

5.4 A possible correlation with compactness?

While this paper was under revision, Läsker et al. (2013) reported detailed dynamical models for an unusually compact elliptical ('b19') with $\sigma \approx 360\,{\rm km\,s}^{-1}$, which appear to require a very heavy IMF ($\alpha \sim 2$). The striking contrast between ESO325−G004 and b19 (which has similar velocity dispersion but approximately seven times higher luminosity surface density) is suggestive of a possible correlation of $\alpha_{\rm MW}$ with galaxy compactness.

Also during the revision of our paper, Conroy et al. (2013b) published average $\alpha_{\rm MW}$ from dwarf-star indicators and dynamical estimates, for a sample of compact elliptical galaxies in SDSS. Their sample definition selects the ∼6 per cent densest early-type galaxies, based on stellar mass surface density. For such galaxies, the contribution of dark matter within the SDSS fibre is sufficiently small to justify assuming that mass follows light in the dynamical models. A consistent trend of increasing $\alpha_{\rm MW}$ with increasing σ is recovered using both methods, but both dynamics and spectral features yield systematically larger $\alpha_{\rm MW}$ for compact ellipticals than found for the CvD12b sample. For example in the highest-σ bin, with $\sigma \approx 300\,{\rm km\,s}^{-1}$, the dwarf-star indicators suggest $\langle\alpha_{\rm MW}\rangle \approx 2.3$, compared to ∼1.7 at the same velocity dispersion in CvD12b.

Both of these recent advances imply that the IMF may vary among galaxies of similar velocity dispersion, in a way that is correlated with galaxy compactness, and hence presumably to the degree of dissipation in the early formation history. Accounting for this modulation may eventually help reconcile ESO325−G004 with results from other studies.

6 CONCLUSIONS

In this paper, we have presented new data on the ESO325−G004 lens system, which demonstrate that *this* giant elliptical galaxy does *not* have a very heavy IMF of the type suggested for similar galaxies in several recent works, in particular T10 and CvD12a. The IMF mass normalization relative to the MW (Kroupa) is $\alpha_{\rm MW} = 1.04 \pm 0.15$, consistent with either a Chabrier or a Kroupa IMF. An IMF heavier than Salpeter ($\alpha_{\rm MW} > 1.55$) is disfavoured at the >99.8 per cent level. This result is robust against a range of possible systematic errors, and to the treatment of dark-matter contributions. Even if we attribute all of the lensing mass to stars, the IMF is lighter than Salpeter at the 98 per cent confidence level.

One explanation for the difference between our result and those favouring heavyweight IMFs is simply that ESO325−G004 is unusual among massive ellipticals: i.e. on average such galaxies have $\alpha_{\rm MW} \approx 2$, but there is some intrinsic scatter around this value, and the closest known strong-lensing elliptical happens to have a much lighter IMF. This possibility cannot be excluded, but we have highlighted two lines of evidence to the contrary. First, the high-σ SLACS lenses *all* have $\alpha_{\rm MW} \approx 2$, apparently with *no* intrinsic scatter (and indeed an observed scatter almost too small to be consistent

with the errors). This suggests that ESO325−G004 differs systematically from the SLACS sample lenses, perhaps due to the different selection/discovery methods involved. Secondly, the strong Na I feature observed in ESO325−G004 suggests that this galaxy is similar to other massive ellipticals in having enhanced dwarf-sensitive spectral features. As we have indicated, a full analysis of these features is required before firm conclusions can be drawn, but since a MW-like IMF does not match the Na I data without extreme Na/Fe ratios, there appears to be some tension between the two methods for this galaxy. We have noted the very recent hints that compact galaxies have heavier IMFs (at given σ) than normal ellipticals, which could help to resolve some of these apparent disagreements.

Observations of a single galaxy cannot provide a definitive answer as to whether massive ellipticals, as a class, formed their stars according to a mass distribution different from that in the MW. Nevertheless, the unique properties of ESO325−G004, the nearest known strong-lensing galaxy, provide an important opportunity to intercompare and calibrate the various methods of constraining the IMF. In future work, we intend to exploit further the dwarf-star indicators measurable both from existing data and from infrared spectroscopy with KMOS (Sharples et al. 2013). We will also use the IFU data to build dynamical models, subject to the lensing constraints, as a further probe of the mass distribution in ESO325−G004.

REFERENCES

Abell G. O., Corwin H. G., Jr, Olowin R. P., 1989, ApJS, 70, 1
Appenzeller I. et al., 1998, Messenger, 94, 1
Arneson R. A., Brownstein J. R., Bolton A. S., 2012, ApJ, 753, 4
Auger M. W., Treu T., Bolton A. S., Gavazzi R., Koopmans L. V. E., Marshall P. J., Bundy K., Moustakas L. A., 2009, ApJ, 705, 1099
Auger M. W., Treu T., Bolton A. S., Gavazzi R., Koopmans L. V. E., Marshall P. J., Moustakas L. A., 2010, ApJ, 724, 511
Barnabè M., Spiniello C., Koopmans L. V. E., Trager S. C., Czoske O., Treu T., 2013, preprint (arXiv:1306.2635)
Bastian N., Covey K. R., Meyer M. R., 2010, ARA&A, 48, 339
Bell E. F., de Jong R. S., 2001, ApJ, 550, 212
Belokurov V. et al., 2007, ApJ, 671, L9
Blumenthal G. R., Faber S. M., Flores R., Primack J. R., 1986, ApJ, 301, 27
Bolton A. S., Burles S., Koopmans L. V. E., Treu T., Moustakas L. A., 2006, ApJ, 638, 703
Bruzual G., Charlot S., 2003, MNRAS, 344, 1000
Cappellari M. et al., 2006, MNRAS, 366, 1126
Cappellari M. et al., 2013, MNRAS, 432, 1862
Carter D., Visvanathan N., Pickles A. J., 1986, ApJ, 311, 637
Cenarro A. J., Gorgas J., Vazdekis A., Cardiel N., Peletier R. F., 2003, MNRAS, 339, L12
Chabrier G., 2003, PASP, 115, 763

Cohen J. G., 1978, ApJ, 221, 788
Conroy C., van Dokkum P., 2012a, ApJ, 747, 69 (CvD12a)
Conroy C., van Dokkum P., 2012b, ApJ, 760, 71 (CvD12b)
Conroy C., Gunn J. E., White M., 2009, ApJ, 699, 486
Conroy C., Graves G. J., van Dokkum P. G., 2013a, preprint (arXiv:1303.6629)
Conroy C., Dutton A., Graves G. J., Mendel J. T., van Dokkum P. G., 2013b, preprint (arXiv:1306.2316)
Couture J., Hardy E., 1993, ApJ, 406, 142
De Lucia G., Blaizot J., 2007, MNRAS, 375, 2
Duffy A. R., Schaye J., Kay S. T., Dalla Vechia C., Battye R. A., Booth C. M., 2010, MNRAS, 405, 2161
Dutton A. et al., 2013, MNRAS, 428, 3183
Faber S. M., French H. B., 1980, ApJ, 235, 405
Ferreras I., La Barbera F., de Carvalho R. R., de la Rosa I. G., Vazdekis A., Falcón-Barroso, Ricciardelli E., 2013, MNRAS, 429, L15
Fioc M., Rocca-Volmerange B., 1997, A&A, 326, 950
Geha M. et al., 2013, ApJ, 771, 29
Gnedin O. Y., Ceverino D., Gnedin N. Y., Klypin A. V., Levine R., Nagai D., Yepes G., 2011, preprint (arXiv:1108.5736)
Johansson P. H., Naab T., Ostriker J. P., 2012, ApJ, 754, 115
Jones D. H. et al., 2004, MNRAS, 355, 747
Jones D. H. et al., 2009, MNRAS, 399, 683
Kalirai J. S. et al., 2013, ApJ, 763, 110
Kochanek C. S., 1991, ApJ, 373, 354
Komatsu E. et al., 2011, ApJS, 192, 18
Koopmans L. V. E., Treu T., Bolton A. S., Burles S., Moustakas L. A., 2006, ApJ, 649, 599
Kroupa P., 2001, MNRAS, 322, 231
La Barbera F., Ferrera I., Vazdekis A., de la Rosa I. G., de Carvalho R. R., Trevisan M., Falcón–Barroso J., Ricciardelli E., 2013, MNRAS, preprint (arXiv:1305.2273)
Laine S., van de Marel R. P., Lauer T. R., Postman M., O'Dea C. P., Owen F. N., 2003, AJ, 125, 478
Läsker R., van den Bosch R. C. E., van de Ven G., Ferreras I., La Barbera F., Vazdekis A., Falcón-Barroso J., 2013, MNRAS, preprint (arXiv:1305.5542)
Le Fevre O. et al., 2003, Proc. SPIE, 4841, 1670
Łokas E. L., Mamon G. A., 2001, MNRAS, 321, 155
Mancone C. L., Gonzalez A. H., 2012, PASP, 124, 606
Maraston C., 2005, MNRAS, 362, 799
Martel A. R. et al., 2004, ApJ, 128, 2758

McConnell N. J., Ma C.-P., Gebhardt K., Wright S. A., Murphy J. D., Lauer T. R., Graham J. R., Richstone D. O., 2011, Nat, 480, 215
Navarro J. F., Frenk C. S., White S. D. M., 1996, ApJ, 462, 563
Neto A. et al., 2007, MNRAS, 381, 1450
Norris M. A., Sharples R. M., Kuntschner H., 2006, MNRAS, 367, 815
Percival S. M., Salaris M., Cassisi S., Pietrinferni A., 2009, ApJ, 690, 427
Remus R.-S., Burkert A., Dolag K., Johansson P. H., Naab T., Oser L., Thomas J., 2013, ApJ, 766, 71
Richard J., Jones T., Ellis R., Stark D. P., Livermore R., Swinbank M., 2011, MNRAS, 413, 643
Salpeter E., 1955, ApJ, 121, 161
Schlafly E. F., Finkbeiner D. P., 2011, ApJ, 737, 103
Sharples R. et al., 2013, ESO Messenger, 151, 21
Smith R. J., Blakeslee J.P., Lucey J. R., Tonry J., 2005, ApJ, 625, L103 (S05)
Smith R. J., Lucey J. R., Hudson M. J., 2007, MNRAS, 381, 1035
Smith R. J., Lucey J. R., Carter D., 2012, MNRAS, 426, 2994
Spiniello C. L., Koopmans V. E., Trager S. C., Czoske O., Treu T., 2011, MNRAS, 417, 3000
Spiniello C., Trager S. C., Koopmans L. V. E., Chen Y. P., 2012, ApJ, 753, L32
Spiniello C., Trager S., Koopmans L. V. E., Conroy C., 2013, preprint (arXiv:1305.2873)
Spinrad H., Taylor B. J., 1971, ApJS, 22, 445
Springel V. et al., 2005, Nat, 435, 629
Taruya A., Takada M., Hamana T., Kayo I., Futamase T., 2002, ApJ, 571, 638
Thomas D., Maraston C., Bender R., 2003, MNRAS, 339, 897
Thomas D., Maraston C., Korn A., 2004, MNRAS, 351, L19
Thomas J. et al., 2011, MNRAS, 415, 545
Treu T., 2010, ARA&A, 48, 87
Treu T., Auger M. W., Koopmans L. V. E., Gavazzi R., Marshall P. J., Bolton A. S., 2010, ApJ, 709, 1195 (T10)
van Dokkum P., Conroy C., 2010, Nat, 468, 940
van Dokkum P. G., Conroy C., 2012, ApJ, 760, 70
Vernet J. et al., 2011, A&A, 536, A105
Wegner G. A., Corsini E. M., Thomas J., Saglia R. P., Bender R., Pu S. B., 2012, AJ, 144, 78
Whitford A. E., 1977, ApJ, 211, 527
Wyse R. F. G., Gilmore G., Houdashelt M. L., Feltzing S., Hebb L., Gallagher J. S., III, Smecker-Hane T. A., 2002, New Astron., 7, 395

This paper has been typeset from a TEX/LATEX file prepared by the author.